Relaxation Dynamics of Ruthenium Complexes in Solution, PMMA and TiO_2 Films: The Roles of Self-Quenching and Interfacial Electron Transfer

Chih-Wei Chang,[†] Chung Kuang Chou,[†] I-Jy Chang,[‡] Yuan-Pern Lee,[†] and Eric Wei-Guang Diau*[,†]

Department of Applied Chemistry and Institute of Molecular Science, National Chiao Tung University, No. 1001, Ta Hsueh Road, Hsinchu 30010, Taiwan, and Department of Chemistry, National Taiwan Normal University, No. 88, Sec. 4, Ting-Chow Road, Taipei 11677, Taiwan

Received: May 18, 2007; In Final Form: July 3, 2007

The relaxation dynamics of two transition-metal complexes, $[Ru(bpy)_3]^{2+}$ and $[Ru(bpy)_3(mcbpy)]^{2+}$, in ethanol solution and in poly(methyl methacrylate) (PMMA) and TiO_2 films have been investigated with time-resolved emission and femtosecond transient absorption spectroscopy. The emission lifetime of a degassed $[Ru(bpy)_3]^{2+}$ solution in ethanol was determined to be 700 ns; to describe the self-quenching kinetics due to aggregation, three decay coefficients, 5.3, 70, and 220 ns, were obtained for the $[Ru(bpy)_3]^{2+}$/PMMA film. The electron transfer through space in a $[Ru(bpy)_3]^{2+}/TiO_2$ film competed with intrinsic intersystem crossing (∼100 fs) and vibrational relaxation (∼6 ps) in solid films. For the $[Ru(bpy)_2(mcbpy)]^{2+}/TiO_2$ film, although the relaxation for electron transfer through bonds was more rapid than electron transfer through space, both processes occur on similar time scales. Through femtosecond transient absorption measurements, we provide important dynamical evidence for the interfacial electron transfer in both forward and backward directions. We conclude that in dye-sensitized solar-cell applications processes for interfacial electron transfer are significant not only through bonds but also through space.

Introduction

Because of the second energy crisis and because of a global thirst for energy, much effort has been devoted to find a cheap, clean, and sustainable source of energy; hence, the applications of solar energy conversion have become increasingly important. For example, the most efficient Si-based solar cell (SC) has attained 24% energy conversion efficiency in the laboratory,[1] and both single-crystalline and polycrystalline Si solar cells have been commercialized. A dye-sensitized solar cell (DSSC) has also attracted much attention as a less expensive alternative to a Si-based SC. Many organic and metallic organic molecules such as coumarins,[2] indolines,[3] porphyrins,[4,5] and conjugated polymers[6] might serve as a sensitizer in a DSSC. The most efficient DSSC is the Grätzel cell developed by Grätzel and co-workers, using a Ru-bipyridyl-based sensitizer with nanocrystalline TiO_2 films in combination; conversion of ∼11% of light to electricity is achieved under AM 1.5 irradiation.[7]

In a Grätzel cell, Ru^{2+} complexes are chemically adsorbed on nanocrystalline TiO_2 films via carboxylic groups (−COOH). Interfacial electron transfer (IET) of two kinds is believed to be critical to the overall efficiency of a DSSC. First, following optical excitation, because the energy of a dye molecule in its excited-state is greater than the energy of the conduction band of TiO_2 nanoparticles, excited molecules inject electrons into the conduction band of TiO_2 films. Second, electrons injected into the conduction band can recombine with the dye cation, thus reducing the dye molecule to the ground state. The rate of charge recombination is reported to range from $\sim\mu s^{-1}$ to $\sim ms^{-1}$, controlled with an externally applied bias[8] or molecular structure,[9] and the rate of electron injection ranges from the femtosecond to the nanosecond time scale;[10−12] the greatest rate was determined to be $>20\ fs^{-1}$ by Wenger et al.[13]

Temporally resolved absorption spectra of $[Ru(bpy)_3]^{2+}$ complex (hereafter abbreviated as Ru-1; its chemical structure appears in Scheme 1) in solution on a femtosecond scale were reported by Damrauer et al.;[14] the earliest dynamics of the excited state were monitored with femtosecond transient absorption spectra. In accordance to those results, the metal to ligand charge transfer ^{3}(MLCT) state was established within ∼300 fs (lifetime ∼100 fs). Bhasikuttan et al.[15] reported femtosecond fluorescence up-conversion results of Ru-1 in CH_3CN; the transients were characterized by a rapid (∼40 fs) intersystem crossing (ISC) and a slow (∼1.0 ps) vibrational cooling. Kallioinen et al.[16] reported that both sample preparation and experimental conditions significantly affect the excited-state dynamics. Here, we report the excited-state relaxation dynamics of Ru-1 either dissolved in ethanol or mixed with poly(methyl methacrylate) (PMMA) as a solid film for comparison.

In the application of a DSSC, a Ru^{2+} complex known as N3 dye is adsorbed on TiO_2 nanoparticles as a thin film via chemical bonds between carboxyl groups and TiO_2 nanoparticles.[7] Hara et al.[17] reported that the injection efficiency increased with the number of carboxyl groups. Because the rate of electron transfer might depend on the number of carboxyl groups, to simplify the problem we used a $[Ru(bpy)_2(mcbpy)]^{2+}$ complex (hereafter abbreviated as Ru-2; its chemical structure is depicted in Scheme 1)[18] in which the electron can inject into the TiO_2 conduction band via only a single carboxyl group. To demonstrate the effect of IET occurring either through space or through chemical bonds, we studied the relaxation dynamics of both Ru-1 and Ru-2 complexes on the surface of a TiO_2 nanocrystalline film

* Corresponding author. E-mail: diau@mail.nctu.edu.tw. Fax: (886)-03-572-3764.
[†] National Chiao Tung University.
[‡] National Taiwan Normal University.

10.1021/jp073843m CCC: $37.00
Published on Web 08/11/2007

SCHEME 1: Chemical Structures of Ru-1 and Ru-2 Complexes

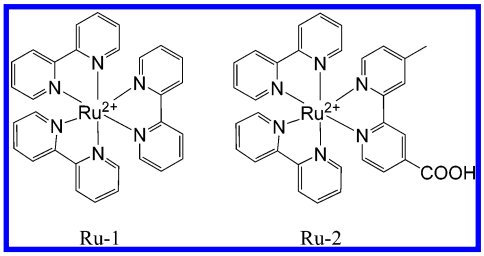

Ru-1 Ru-2

using the techniques of femtosecond optically gated (FOG) and transient absorption (TA) spectroscopy with a time resolution ~100 fs.

Experimental Procedures

Sample preparation. Ru-1 and ethanol (Aldrich) were used without further purification; Ru-2 was synthesized by a standard procedure.[19] To prepare PMMA thin films, we dissolved Ru-1 and PMMA in $CHCl_3$, mixed them homogenously, and spin-coated the solution onto a glass substrate. TiO_2 nanoparticle films were prepared with a procedure reported elsewhere.[20] The thickness of the TiO_2 film was determined to be 6 μm; the particle size was 15−20 nm.[5] Thin films of Ru-1 and Ru-2 on TiO_2 were prepared by immersing a TiO_2 film into Ru-1/$CHCl_3$ solution (10^{-4} M) and Ru-2/ethanol solution (10^{-4} M) for 8 h. After immersion, the Ru-2/TiO_2 film was washed with clean ethanol to remove all dye molecules not chemically adsorbed onto the surface of the TiO_2 film. The Ru-1/TiO_2 film was used without washing; because no chemical bond was formed between Ru-1 and TiO_2, washing caused loss of all dye molecules. Both Ru-1/TiO_2 and Ru-2/TiO_2 films were exposed to the ambient atmosphere for spectral and kinetic measurements.

Steady-State Spectral Measurements. UV/visible absorption spectra of samples in solution and thin films were measured with a standard spectrophotometer (Cary 50, Varian). Emission spectra were obtained with a composite CCD spectrometer (USB2000FLG, Ocean Optics) with an excitation source shared with the same femtosecond laser system as used in time-resolved measurements.

Picosecond Emission Decay Measurements. Picosecond temporally resolved spectra were recorded with a time-correlated single-photon counting (TCSPC) system (Fluotime 200, PicoQuant)[21] with the same excitation source as used in femtosecond emission experiments. The rate of repetition of the laser pulse was fixed at 500 kHz with a pulse picker (Model 9200, Coherent). The laser frequency was doubled with a harmonic generation system (Model 9300, Coherent) and used for excitation. A beam splitter served to split a small portion of the laser pulse to trigger a reference photodiode (TDA200, PicoQuant) that generated the synchronization signal for the TCSPC system. The excitation pulse was focused onto the sample holder (for ethanol a 1 cm cuvette but for solid films a rotating sample holder) with a lens. A lens collected emission emitted from the sample at a right angle. An iris attenuated the intensity of the detected signal; the polarization of the detected emission relative to the excitation laser pulse was set at 54.7° with a polarizer. A double monochromator compensated the group-velocity dispersion of emission and selected the detection wavelength; the resolution was 8 nm with a slit of width 1 mm. For data acquisition, a microchannel plate photomultiplier was connected to a computer with a TCSPC-module card (SPC-630, Becker and Hickl GmbH). The full width at half-maximum (FWHM) of the instrument response function (IRF) was 50 ps, as measured with scattered light at the laser excitation wavelength.

All spectral measurements were performed near 295 K under the condition of purging fresh N_2 gas.

Femtosecond Emission Decay Measurements. Femtosecond up-conversion signals were recorded with an optically gated system (FOG100, CDP) in combination with a mode-locked Ti:sapphire laser (Mira 900D, Coherent) described in detail elsewhere.[5a,22] A brief summary follows. The femtosecond laser system generates output pulses of duration ~150 fs (FWHM of autocorrelation) at a repetition rate 76 MHz. The spectral bandwidth is 10−12 nm and is tunable from 700 to 1000 nm. The frequency of the laser pulse is doubled with a Beta-Barium Borate (BBO) crystal (type I) and is used for excitation (pump); the residual fundamental pulse that serves as a probe beam is split from the pump beam with two dichroic beam splitters. The intensity of the excitation beam (λ_{ex} = 430 nm) was appropriately attenuated (laser power ~30 mW or ~0.4 nJ pulse^{-1}) and focused onto a rotating sample cell (beam size ~20 μm). Emission was collected with two parabolic mirrors and focused onto a BBO crystal (type I). The gate pulse (probe) was also focused on the BBO crystal for sum-frequency generation (up-conversion). The delay between the gate pulse and emission was controlled with a stepping translational stage. The up-conversion signal was collected with a lens and separated from interference with an iris, a band-pass filter, and a double monochromator in combination, then detected with a photomultiplier (R1527P, Hamamatsu) that was in turn connected to a computer-controlled photon-counting system. A Berek polarization compensator controlled the polarization of the pump beam; the relative polarization between pump and probe beams was fixed at 54.7°.

Femtosecond Transient Absorption Measurements. Femtosecond transient absorption spectra were recorded with a pump−probe spectrometer (ExciPro, CDP) in combination with an ultrafast amplified laser system. The amplified laser pulses were obtained from a regenerative amplifier (Legend-USP-1K-HE, Coherent) seeded with a mode-locked Ti:sapphire laser system (Mira-Seed/ Verdi V5, Coherent) and pumped with a 1-kHz Nd:YLF laser (Evolution 30, Coherent). The laser pulses are centered at 800 nm with an average energy 2.5 mJ pulse^{-1}. The FWHM of the amplified pulses (~60 fs) was determined by a single-shot autocorrelator (Coherent). The amplified pulse was equally split to pump two optical parametric amplifiers (OPerA-F, Coherent) in combination with harmonic generations (SHG, THG, and FHG), sum-frequency generation (SFG), and difference-frequency generation modules, which provide tunable femtosecond pulses in the wavelength range 240 nm−10 μm.

Figure 1 shows the optical layout of the femtosecond pump−probe TA spectrometer. Basically, the dye molecules in an electronic excited-state can be prepared by an excitation pulse (Pump); the resulting transient species and their relaxation dynamics can be monitored by a probe pulse (Probe). The polarization of the excitation pulse was controlled with a Berek compensator (B1), and the pump beam was focused onto the rotating sample cell containing the solution or thin-film samples. For single-wavelength kinetic measurements, the probe pulse was generated with the OPA/wavelength converter; for transient absorption spectral measurements, the white-light (WL) continuum was produced on focusing the residual amplified pulse (800 nm) on a continuous water-flow cell (WL cell). To record transient absorption spectra with and without the excitation pulses, we used a chopper to modulate the excitation pulse. The

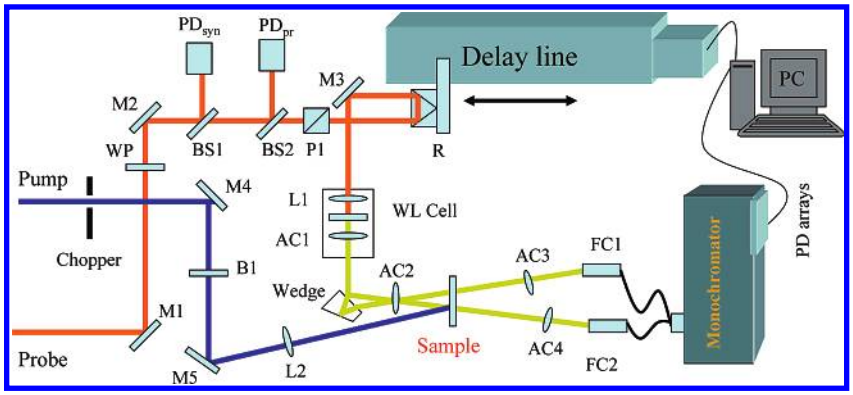

Figure 1. Optical layout of the femtosecond transient absorption spectrometer. M1−M5, gold or aluminum mirrors; BS1 and BS2, beam splitters; Wedge, wedge prism; B1, Berek compensator; WP, half-wave plate; Pl, polarizer; L1 and L2, lens; AC1−AC4, achromatic lens; FC1 and FC2, optical fiber couplers; PD, photodiode; R, retro-reflector. For single wavelength measurements, the white-light (WL) cell was removed, and both FC1 and FC2 were replaced with two photodiodes.

probe beam was first split into a small portion via BS1 to synchronize the chopper with a photodiode (PD_{syn}) and then split into another small portion via BS2 to monitor the stability of the probe pulse by another photodiode (PD_{pr}). The vertical polarization of the probe pulse was selected with a polarizer (P1), and the intensity of the probe pulse was controlled on rotating a half-wave plate (WP) in the optical path ahead of P1. The probe beam was separated into two parts with a wedge prism; one part of the beam was focused on the sample cell via AC2 and overlapped with the excitation beam to give a probe signal (I_{pr}); the other part of the beam was also focused via AC2 onto another place of the sample cell to serve as a reference signal (I_{ref}). For the one-color probe, the I_{pr} and I_{ref} signals were recorded with two Si photodiodes (not shown); for the WL probe, the $I_{pr}(\lambda)$ and $I_{ref}(\lambda)$ signals were collected with two optical fiber couplers (FC1 and FC2) connected to a monochromator equipped with two Si photodiode arrays (2 × 1024 channels). At a particular temporal delay, the difference of optical density between $I_{pr}(\lambda)$ and $I_{ref}(\lambda)$ is expressible in the following equation according to Beer's law:

$$\Delta OD(\gamma) = \log \frac{I_{ref}(\lambda)}{I_{pr}(\lambda)} \quad (1)$$

By varying the temporal delay between the excitation and the probe pulses via a stepping translational stage (delay line), we obtained a three-dimensional transient absorption profile (ΔOD vs λ and t). The relative polarization between the excitation and probe pulses was fixed at the magic angle (54.7°).

To obtain further evidence for IET on solid films, we performed femtosecond kinetic measurements of anisotropy using the single-wavelength pump−probe method with excitation and detection wavelengths fixed at 450 and 900 nm, respectively. Basically, the TA signals of parallel polarization, $\Delta OD_{//}(t)$, and perpendicular polarization, $\Delta OD_{\perp}(t)$, were measured separately. The temporally resolved anisotropy is evaluated with the following equation:

$$r(t) = \frac{\Delta OD_{//}(t) - \Delta OD_{\perp}(t)}{\Delta OD_{//}(t) + 2 \times \Delta OD_{\perp}(t)} \quad (2)$$

The denominator represents the total TA signal equal to three times the TA signal measured at the magic-angle condition that produces no preferential orientation. The TA signals at a magic angle are thus obtained with the following equation:

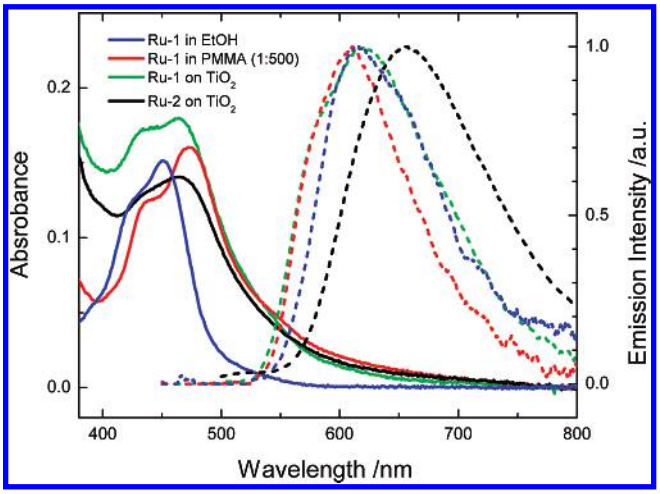

Figure 2. Steady-state spectra of Ru-1 and Ru-2 in various environments with solid curves for absorption and broken curves for emission. Glass served as the reference sample for absorption spectra of PMMA and TiO_2 films; the excitation wavelength of emission spectra was fixed at 430 nm.

$$\Delta OD(t) = \frac{\Delta OD_{//}(t) + 2 \times \Delta OD_{\perp}(t)}{3} \quad (3)$$

Results

Steady-State Spectra. Figure 2 shows steady-state spectra of Ru-1 and Ru-2 in various environments. Although the shapes of the absorption spectra of the Ru-1 samples are similar, two features of the spectra are notable: the absorption maxima at 425 and 450 nm in solution become shifted to 435 and 465 nm in solid films, and the absorption spectra in solid films have a long tail as far as ~700 nm.

All emission spectra in Figure 2 were excited at 430 nm. For an ethanol (EtOH) solution, the spectrum featured an emission maximum about 620 nm; in a PMMA film, the emission spectrum was blue-shifted to 610 nm. For a Ru-1/TiO_2 film, the spectrum was similar to that for an ethanol solution but became significantly broadened. In Ru-2/TiO_2 films, the spectrum was red-shifted to 660 nm.

Picosecond Emission Decays. To obtain further information about the excited-state of Ru-1 or Ru-2 in various environments, we measured temporally resolved emission decays of a degassed Ru-1/EtOH solution, a Ru-1/PMMA film, a Ru-1/TiO_2 film, and a Ru-2/TiO_2 film using TCSPC. Each sample was measured on two time scales; transients in ranges 0−30 ns and 0−1000

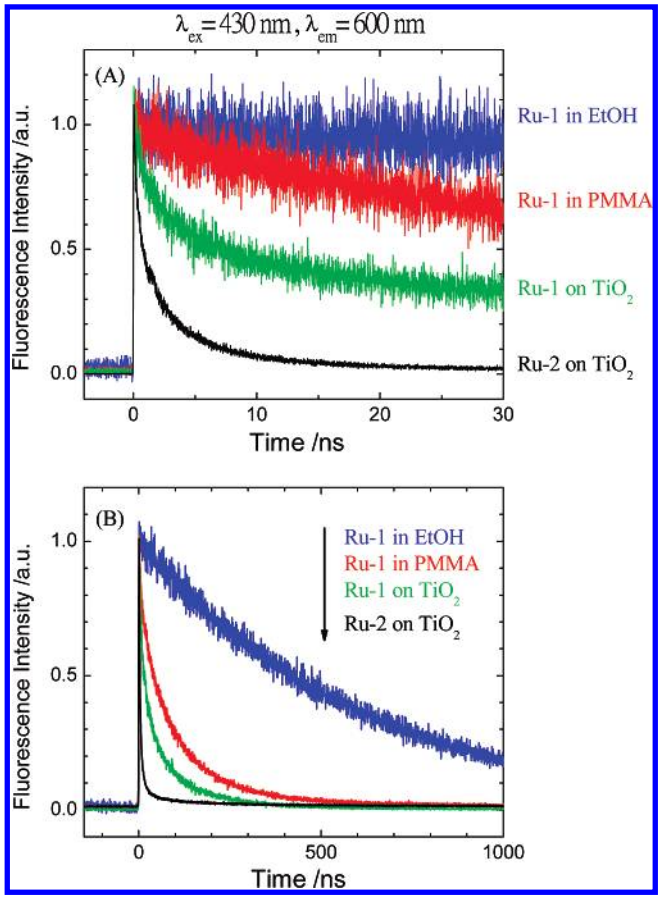

Figure 3. Picosecond transients of Ru-1 and Ru-2 in various environments; excitation and emission wavelengths were fixed at 430 and 600 nm, respectively. (A) Spectra between 0 and 30 ns, FWHM of the IRF is ~50 ps; (B) spectra between 0 and 1000 ns, FWHM of the IRF is ~1.2 ns.

TABLE 1: Time Coefficients Obtained from the Kinetic Fits of Ru-1 and Ru-2 in Various Environments[a]

	Ru−1 in ethanol	Ru−1 in PMMA	Ru-1 on TiO_2	Ru-2 on TiO_2
TCSPC[b]	$\tau = 700$ ns	$\tau_1 = 5.3$ ns	$\tau_1 = 1.3$ ns	$\tau_1 = 0.34$ ns
		$\tau_2 = 70$ ns	$\tau_2 = 20$ ns	$\tau_2 = 2.1$ ns
		$\tau_3 = 220$ ns	$\tau_3 = 120$ ns	$\tau_3 = 7.2$ ns
				$\tau_4 = 150$ ns
FOG[c]	$\tau_1 = 0.14$ ps	$\tau_1 = 0.14$ ps	$\tau_1 = 0.12$ ps	$\tau_1 = 0.1$ ps
	$\tau_2 = 3.8$ ps	$\tau_2 = 6.0$ ps	$\tau_2 = 3.0$ ps	$\tau_2 = 1.9$ ps
TA[c]	$\tau_1 = 0.15$ ps		$\tau_1 = 0.1$ ps	$\tau_1 = 0.1$ ps
	$\tau_2 >$ ns		$\tau_2 \sim 70$ ps	$\tau_2 = 23$ ps

[a] For emission decays, the excitation and emission wavelengths were 430 and 600 nm, respectively; for transient absorption decays, the pump and probe wavelengths were 450 and 900 nm, respectively. [b]The transients were fitted with multiple functions for parallel exponential decays. [c]The transients were fitted with a consecutive model $A \xrightarrow{\tau_1} B \xrightarrow{\tau_2} C$.

ns are shown in Figure 3A,B, respectively. For the degassed Ru-1/EtOH solution, the phosphorescent decay was fitted with a single-exponential decay with time coefficient 700 ns.

To investigate the effect of a rigid environment without interference from electron-transfer dynamics, we mixed Ru-1 with PMMA. The phosphorescent decay of Ru-1 in PMMA films is describable with a multiexponential decay; three time coefficients obtained from fitting the data are listed in Table 1. The phosphorescent decay of Ru-1 in a PMMA thin film was more rapid than that in degassed ethanol solution to be discussed in the next section. To test the effect of electron transfer through

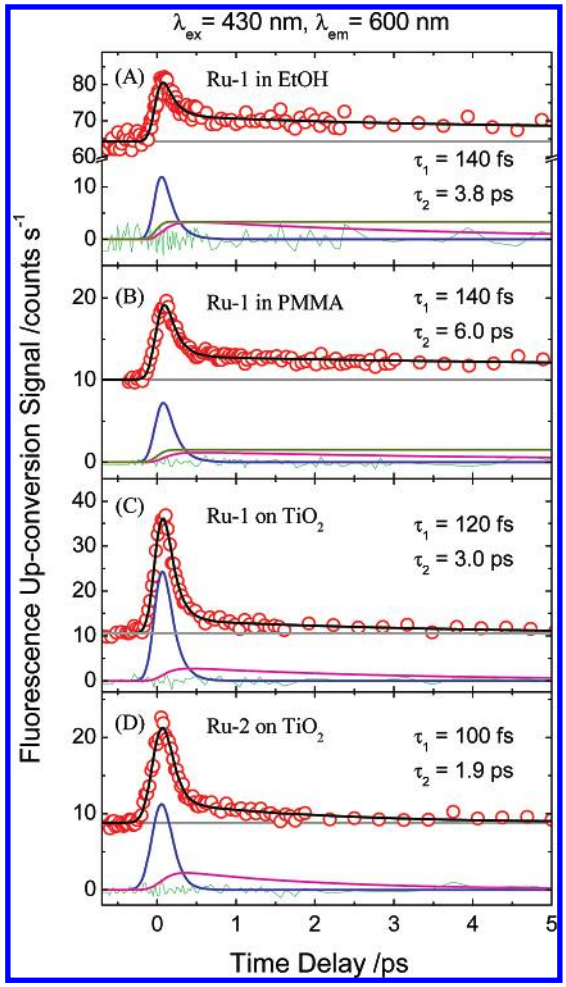

Figure 4. Femtosecond transients of Ru-1 and Ru-2 in various environments with time coefficients from the kinetic fits indicated. The transients were fitted according to a consecutive kinetic model, $A \xrightarrow{\tau_1} B \xrightarrow{\tau_2} C$. The solid black curves are theoretical fits with residues shown as green traces; the blue and magenta curves under each transient are deconvoluted components corresponding to *A* and *B*, respectively; the dark yellow curves in (A) and (B) represent the offset components that are negligible in (C) and (D).

space from Ru-1 to TiO_2 nanoparticles, we coated Ru-1 on TiO_2 films without washing. As shown in Figure 3B, the emission transient is quenched more rapidly than that of Ru-1 in a PMMA film; the fitted parameters are listed in Table 1. This result indicates that interfacial electron transfer through space quenches efficiently the phosphorescence in the nanosecond range. In the transient of a Ru-2/TiO_2 film, an additional 0.34 ns component appeared, and other nanosecond components were substantially quenched. To resolve the dynamics for the subnanosecond components, we measured the temporally resolved emission signals using up-conversion; the results are presented in the next section.

Femtosecond Emission Decays. As shown in Figure 4 with the improved temporal resolution in our femtosecond experiments, we were able to observe additional ultrarapid relaxation processes that were indiscernible in the transients obtained from the TCSPC method. Because of a limited rate of repetition of laser pulses (76 MHz, corresponding to a 13.2 ns separation between two pulses), all femtosecond transients of Ru-1 and Ru-2 are constructed on a constant background (~60 counts s^{-1} in solution samples and ~10 counts s^{-1} in thin-film samples), which derives from the long-lived triplet state observed in the TCSPC experiments. In Figure 4, all transients

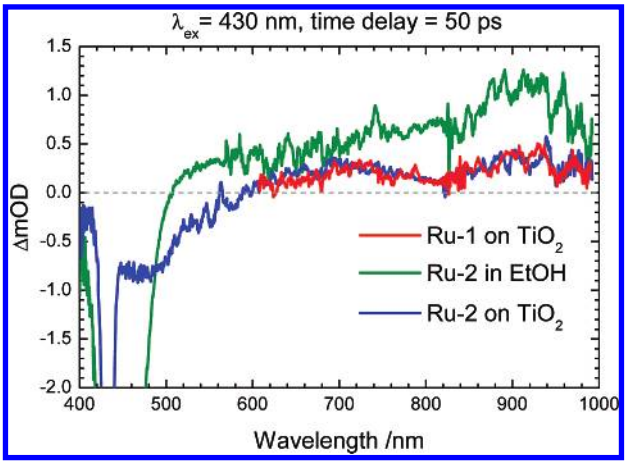

Figure 5. Transient absorption spectra of Ru-2 in ethanol solution and Ru-1 and Ru-2 on TiO_2 films obtained with excitation fixed at 430 nm and a delay 50 ps.

were fitted with a consecutive model, $A \xrightarrow{\tau_1} B \xrightarrow{\tau_2} C$; the time coefficients from the kinetic fits are shown in Table 1. For samples in ethanol and PMMA (Figure 4A,B), the transients appear similar; both feature a rapid femtosecond decay (140 ± 20 fs; the uncertainty represents one standard error of the fit) and a picosecond component (3.8 ± 1.3 ps in ethanol and 6.0 ± 1.0 ps in PMMA); the offset that appears in the transients corresponds to the nanosecond components observed from the TCSPC measurements. In Figure 4C, the time coefficients from the kinetic fits are 120 ± 10 fs and 3.0 ± 1.2 ps. The offset that appears in the transients of Ru-1 in ethanol and the PMMA film was significantly quenched for a Ru-1/TiO_2 film, which indicated an additional nonradiative process to be involved. Similar relaxation dynamics are shown in Figure 4D ($\tau_1 = 100$ ± 10 fs and $\tau_2 = 1.9 \pm 0.4$ ps); the picosecond component in the Ru-2/TiO_2 film decayed more rapidly than that in the Ru-1/TiO_2 film. This phenomenon is attributed to IET that is more rapid through bonds than through space. We expect for Ru-2 on a TiO_2 film that IET through both bonds and space are involved.

Femtosecond Transient Absorption Spectra. In the previous section, we reported that IET through both bond and space would quench the excited-state population efficiently. To provide additional evidence for IET, we conducted measurements of femtosecond transient absorption for Ru-1 and Ru-2 dissolved in ethanol solutions and adsorbed on TiO_2 films. The transient absorption spectra of the Ru-1/TiO_2 film, the Ru-2/TiO_2 film, and the Ru-2/EtOH solution are shown in Figure 5; the delay between pump and probe beams was fixed at 50 ps. In Figure 5, the negative signals at ~430 nm were caused by the scattering of the excitation pulse that makes I_{pr} greater than I_{ref}; similarly the negative signals in the region 400−500 nm (for Ru-2 in ethanol) and 400−600 nm (for Ru-2 on TiO_2) were caused by the ground-state depletion via the excitation pulse that makes I_{pr} greater than I_{ref} when the delay is positive. The latter phenomenon is consistent with the steady-state absorption spectra of Ru-2 in ethanol and on TiO_2 shown in Figure 2.

For Ru-2 in ethanol solution, we observed a broad absorption band above 500 nm corresponding to the long-lived excited-state of the molecule. For Ru-2 on TiO_2, we observed two broad absorption bands centered at 700 and 900 nm, respectively. The result of the Ru-1/TiO_2 film is similar to that of the Ru-2/TiO_2 film but both spectra differ from that observed in solution. As is discussed below, we assign the transient signals observed at 50 ps on solid films (no emissions were observed in Figure 4

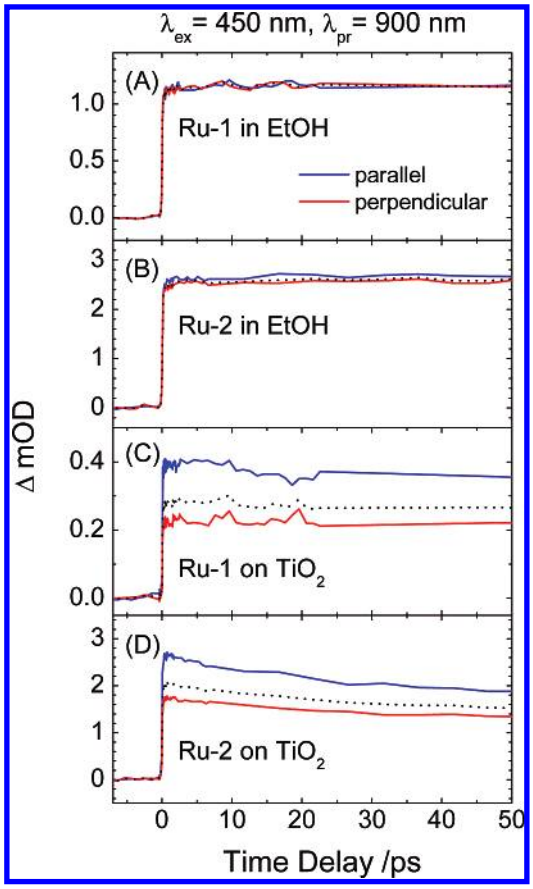

Figure 6. Single-wavelength transient absorption signals of Ru-1 and Ru-2 in ethanol and TiO_2 obtained at excitation and probe wavelengths 450 and 900 nm, respectively. The relative polarization of the excitation beam with respect to the probe beam was fixed at the parallel (blue curves) and perpendicular (red curves) conditions.

on that time scale) to be due to the ionic species that were produced after electron injection from the dye molecules into the TiO_2 nanoparticles of the solid films. IET therefore occurred not only on Ru-2/TiO_2 film through chemical bonds but also on both films through space.

Femtosecond Transient Absorption Anisotropy Kinetics. Figure 6A−D show the single-wavelength TA decays at parallel (blue curves) and perpendicular (red curves) polarizations for Ru-1 and Ru-2 in ethanol solutions (A and B) and on TiO_2 films (C and D); the time-resolved anisotropies are obtained according to eq 2; the corresponding results are shown in Figure 7. For Ru-1 and Ru-2 in solutions, the observed anisotropies are not only independent of time but also nearly zero. These results are consistent with the result of Wallin et al.[23] in which the zero transient absorption anisotropy of Ru-1 in acetonitrile was assigned to the ultrarapid interligand energy randomization in the triplet MLCT state. When Ru-1 and Ru-2 adsorbed on TiO_2, however, both anisotropy decays show a similar behavior: an initial anisotropy ~0.15 followed by a slow decay to an asymptotic level ~0.12 (Figure 7). Apparently, the depolarization behavior of Ru-1 and Ru-2 on TiO_2 films is quite different from that in ethanol; we discuss this point in the next section.

The single-wavelength TA decays at the magic-angle condition are obtained according to eq 3; the results are shown as dotted curves in Figure 6. The transients exhibit no apparent decay for both Ru-2 and Ru-1 in ethanol whereas a slow decay was observed for both Ru-2 and Ru-1 on TiO_2. The data were fitted with a consecutive kinetic model and the corresponding fitted results are shown in Figure 8A−D. For solution data

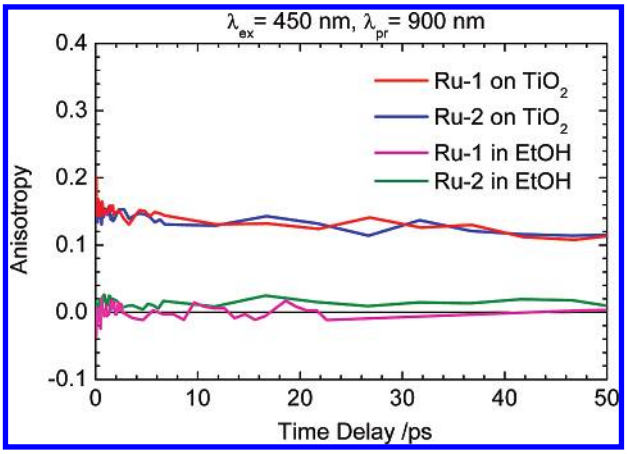

Figure 7. Single-wavelength transient absorption anisotropy decays of Ru-1 and Ru-2 in ethanol solutions and on TiO_2 films constructed from Figure 6 according to eq 2. The excitation and probe wavelengths were fixed at 450 and 900 nm, respectively.

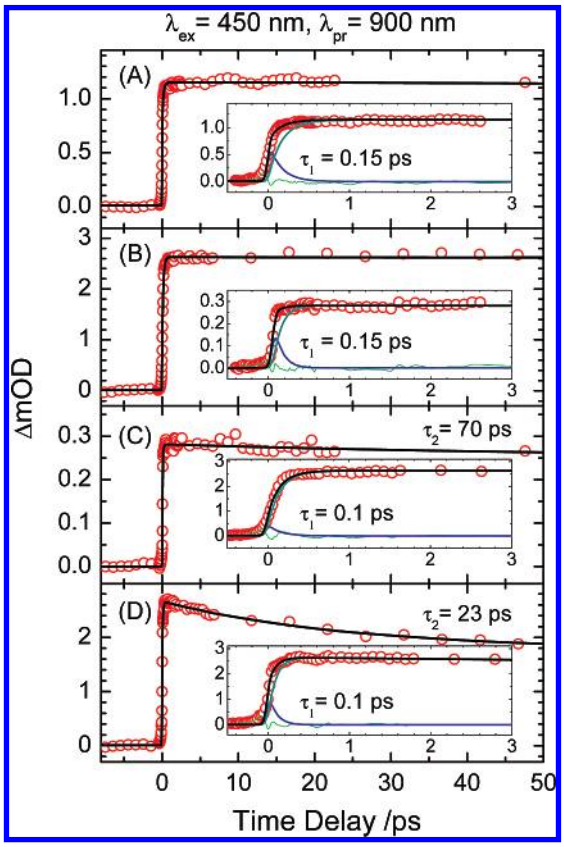

Figure 8. Single-wavelength transient absorption decays of Ru-1 and Ru-2 in ethanol solutions and on TiO_2 films constructed from Figure 6 according to eq 3. For Ru-1 and Ru-2 in ethanol solutions (A and B), the transients were fitted with a consecutive kinetic model, $A \xrightarrow{\tau_1} B \xrightarrow{\tau_2} C$, with τ_2 set to infinity; the transients of Ru-1 and Ru-2 on TiO_2 films (C and D) were fitted with a consecutive model, $A \xrightarrow{\tau_1} B \xrightarrow{\tau_2} C \xrightarrow{\tau_3} D$, with τ_3 set to infinity. Insets of each subfigure show the corresponding transients in the 0−3 ps region.

(Figure 8A,B), the transients feature a rapid-decay component ($\tau_1 = 150$ fs) followed by a long-lived component of which the decay coefficient is indeterminate on the observed 50 ps scale ($\tau_2 >$ ns). For thin-film data (Figure 8C,D), we observed a rapid-decay component ($\tau_1 = 100$ fs) for both compounds. Furthermore, a slow-decay component that was absent from the solution data appears; the second decay coefficients (τ_2) were evaluated to be ~70 ps and 23 ± 5 ps for the Ru-1/TiO_2 and the Ru-2/TiO_2 films, respectively. The time coefficients of both solution and thin-film samples are summarized in Table 1 for comparison.

Discussion

Formation of Aggregates in Solid Films. In a preceding section, we report that the absorption spectra of Ru-1 in ethanol solution feature two intense maxima at 425 and 450 nm. These signals originate from transitions with transfer of charge from metal to ligand corresponding to the ^{1}MLCT state.[24] Red-shifted spectra indicate formation of aggregates when Ru-1 or Ru-2 molecules were dispersed in PMMA or adsorbed on TiO_2 films. The Mie-scattering spectral feature that extended to ~700 nm also supports the hypothesis of aggregate formation in PMMA or TiO_2 films.[25]

The emission spectrum of Ru-1 in a PMMA film is blue-shifted relative to that in ethanol solution because the relaxation through intramolecular motions involved in solution was restricted in a PMMA thin film. In Ru-2/TiO_2 films, the bathochromic shift of the emission spectrum originates from interaction between a carboxylic acid group and TiO_2 nanoparticles, which extend the length of π-orbital conjugation of the Ru-2 complex.

Nonradiative Relaxation in Solution and in Solid Films. The phosphorescence of a degassed Ru-1/ethanol solution shows a single-exponential decay with a lifetime 700 ns. Because there is no electron transfer in Ru-1 solution, this decay character indicates that deactivation occurs only through ISC from ^{3}MLCT to the ground state. In accordance to similar experiments performed by Houten et al.[26] and by Fan et al.,[27] the phosphorescence lifetime of Ru-1 in a N_2-saturated aqueous solution is 580 ns, which is less than the value that we obtained. A possible reason for this difference is their use of light at 337 nm (from a nanosecond nitrogen laser) to excite the molecules, whereas we used light at 430 nm (from a femtosecond Ti:sapphire laser). In their case, because the molecule has greater available energy, another nonradiative process might occur that decreases the lifetime of the ^{3}MLCT state. Another possible reason for the difference is the solvent used in those two experiments (H_2O versus ethanol), which might also affect the dynamics that we observed.[24]

The main difference between Ru-1 in PMMA and ethanol solution is that intramolecular motion with large amplitude is inhibited in a PMMA film. According to previous work,[22,28−30] in many cases intramolecular motions lead to a nonradiative process, which would quench efficiently the fluorescence (or phosphorescence). For this reason, we expected the phosphorescence lifetime of Ru-1 in PMMA film to be greater than that of Ru-1 in ethanol solution, but we observed the reverse. Although we cannot exclude the possibility that some intramolecular motion might still be involved for the former, there must exist other factors that cause the quenching of the phosphorescence of the former. Because some Ru-1 aggregates exist in a PMMA film, we assign the multiexponential decay of the transient of the Ru-1/PMMA film to arise from the self-quenching of heterogeneous Ru-1 aggregates; the rate of quenching varies from 220 to 5 ns^{-1}, controlled by the extent of aggregation.

To investigate further the self-quenching effect due to aggregation, we spin-coated the pure Ru-1 compound without mixing with PMMA on a quartz plate and measured its emission transients for comparison. Figure 9 shows the results on two time scales. Two dynamical features regarding the effect of self-quenching emerge. First, the nonradiative decay of the pure Ru-1

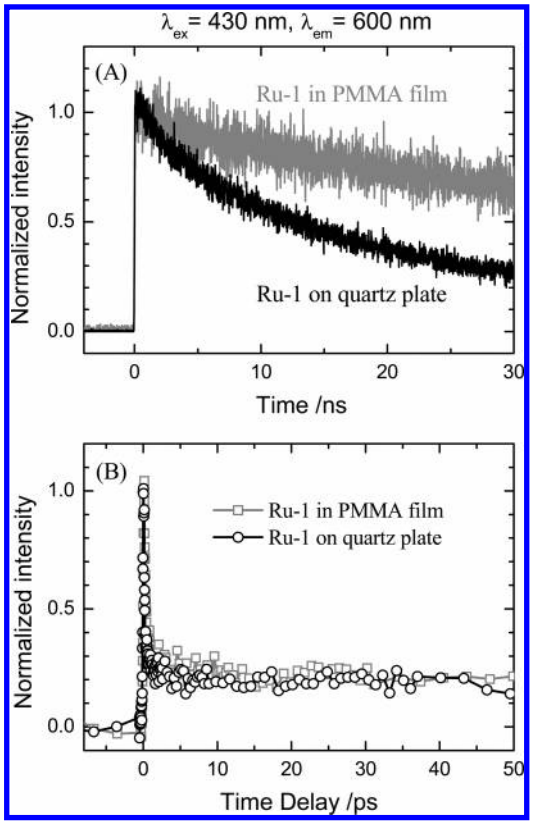

Figure 9. Comparison of time-resolved emission profiles between Ru-1/PMMA and pure Ru-1 solid films on (A) the nanosecond scale with the TCSPC method and (B) the picosecond scale with the FOG method.

solid film is more rapid than that of Ru-1 in a PMMA film on a nanosecond scale (Figure 9A), due to the effect of tighter aggregation of the former than the latter. This result is consistent with that of Ogawa et al.[31] who adsorbed Ru-1 on mesoporous silica and reported that self-quenching in aggregated Ru-1molecules depends on the proportion of the adsorbed dye molecule; the greater the proportion of adsorbed dyes, the more rapid is the decay. Second, however, Figure 9B shows the similarity of the two transients on a picosecond scale, indicating that the nonradiative relaxation of self-quenching is less likely to occur on a time scale competing with other relaxation processes, as we discuss in detail in the following sections.

Through-Space Electron Transfer between Ru-1 and TiO_2. For a Ru-1/TiO_2 film, the phosphorescence of Ru-1 was quenched to a greater extent than for a Ru-1/PMMA film. This phenomenon indicates that electron transfer between Ru-1 and TiO_2 nanoparticles should be considered exclusively for the Ru-1/TiO_2 sample. Both time-resolved and photocurrent measurements have produced evidence of electron transfer through space.[31−34] Hashimoto et al.[32] who performed a similar experiment reported that the luminescence decay of Ru-1 on TiO_2 was fitted with a sum of four exponential components; each decay component was attributed to a separate binding site in the TiO_2 films, which have varied rates of electron transfer. Because the rate of electron transfer through space depends on the distance between donor and acceptor,[35] the various binding sites might also be considered. We thus concluded that the luminescence of Ru-1 was quenched via electron transfer through space, and the multiexponential decay that we observed is attributed to molecules with varied distances between donor and acceptor. The phosphorescence decay that we observed is the statistical average of all dye molecules adsorbed on TiO_2 nanoparticles, causing the rate of electron transfer to have a broad distribution. For this reason, the components that are required to fit the transient are considered to constitute a statistically averaged result of an averaged distance between a Ru-1 complex molecule and a TiO_2 nanoparticle.

Through-Bond Electron Transfer between Ru-2 and TiO_2. The results in Figure 3 show that the relative amplitudes of nanosecond components in Ru-2-sensitized TiO_2 films were decreased beyond those of the Ru-1/TiO_2 films. This phenomenon indicates that besides self-quenching and electron transfer through space another channel quenched the luminescence efficiently. Because the only difference between Ru-1 and Ru-2 is the carboxyl group, the subnanosecond component that we observed in the Ru-2/TiO_2 sample is attributed to electron transfer through a chemical bond. In the following section, we discuss our femtosecond FOG and TA results to elucidate the ultrarapid relaxation of the through-bond IET between Ru-2 and TiO_2.

Femtosecond Relaxation Dynamics from Emission Decays. Consistent with Damrauer et al.[14] and with Bhasikuttan et al.,[15] we attribute the 140 fs and 3.8 ps components observed in the Ru-1/ethanol solution (Figure 4A) to the ^{1}MLCT → ^{3}MLCT ISC and vibrational cooling, respectively. In Bhasikuttan's results, the signal returned to the background level after 1.2 ps, and no offset appeared in their transients. Because wavelengths of excitation (430 versus 410 nm) and emission (600 versus 575 nm) are similar in both experiments, this discrepancy should not originate from those experimental conditions. A possible reason for this discrepancy is that the quality of Bhasikuttan's data[15] is inadequate to distinguish the offset that we observed. In a PMMA film (Figure 4B), the emission transient was similar to that in ethanol solution; we thus used the same model as for Ru-1 in ethanol solution to explain the excited-state dynamics in a PMMA film. Because we observed no extra dynamical effect accelerating the emission decay on this time scale, the self-quenching caused by aggregated molecules is expected to be slow, as mentioned previously (Figure 9). The first component decays similarly in both samples (∼140 fs), which reflects the ultrarapid nature of ISC in Ru-1. The decay of the second component is, however, slower in PMMA film (6 ps) than in ethanol solution (3.8 ps). Because vibrational cooling relates to energy exchange between solute and solvent molecules,[36] this result indicates that the energy exchange in PMMA solid films is less efficient than that in ethanol solution.

In the Ru-1/TiO_2 films, the offset that appears in the transients of a Ru-1/ethanol solution and a PMMA film is significantly quenched. From emission decays of Ru-1 in a PMMA thin film, we recognized that the effect of self-quenching due to aggregation on this time scale was insignificant. In Figure 10, we show the results of a control experiment with two Ru-1/TiO_2 films for which the proportions of Ru-1 molecules coated on TiO_2 films differed: the amount of dye adsorbed in Film 1 is three times that in Film 2 at the wavelength of excitation (λ_{ex} = 430 nm). We found that the ultrarapid decay components are similar in both films, but Film 1 features a prominent offset component that is absent for Film 2. This control experiment indicates that self-quenching due to aggregation at a large molecular concentration (as in Film 1) occurs on the nanosecond time scale, which is consistent with the result of Ru-1 coated on a quartz plate shown in Figure 9. The emission quenching that we observed in Film 2 is thus attributed to electron transfer through space from Ru-1 to TiO_2 nanoparticles.

Our real-time observation indicates that an electron transfer through space might be efficient because the two time coefficients increase to 120 fs and 3.0 ps. Such a dynamical effect becomes more pronounced when the molecules (Ru-2) are

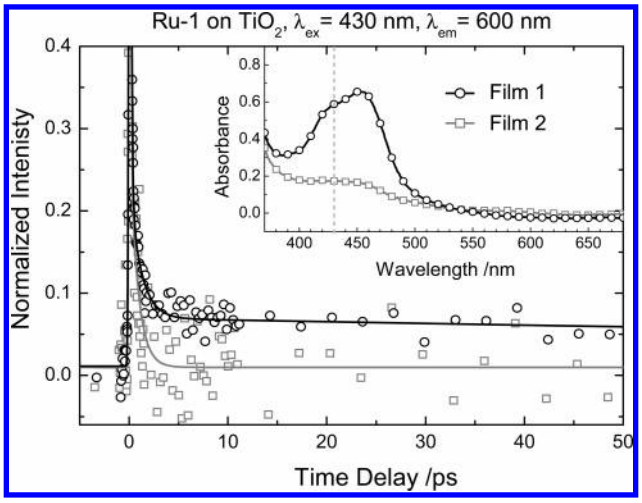

Figure 10. Femtosecond transients (symbols) and fitted results (solid curves) for Ru-1/TiO_2 samples with two different concentrations of dye molecules adsorbed in solid films; the corresponding absorption spectra are shown in the inset.

chemically bonded to the surface of TiO_2; the reduction in both time coefficients (100 versus 120 fs and 1.9 versus 3.0 ps) reflects the involvement of interfacial electron transfer through chemical bonds in addition to transfer through space. We expect that both dynamical processes, electron injection through a bond and through space, would compete with the intrinsic ISC and the vibrational relaxation involved in the least energetic excited state (i.e., ^{3}MLCT).

Femtosecond Relaxation Dynamics from Transient Absorption Decays. Figure 5 shows a significant discrepancy between the TA spectra of the thin-film samples and those of the solution samples, indicating that the transient species observed in solid films differ from those observed in solutions. This observation is further confirmed by the single-wavelength time-resolved anisotropy measurements that demonstrate the depolarization behavior of the thin-film samples to be entirely different from that of the solution samples (Figure 7). For those solution samples, the TA signals (Figure 8A,B) show apparently a rising behavior to a constant level that persists long due to a long-lived ^{3}MLCT state that was produced from the ^{1}MLCT state in the observed 150 fs. The vibrational cooling component discernible in the emission decay (Figure 4A) here becomes difficult to resolve in the TA transients because of a much broader detection window involved for the latter.

In contrast, the emission transients in solid films (Figure 4C,D) decay to a background level whereas the TA transients (Figure 8C,D) rise to a plateau level and then decay to a constant level. We observed emission because the dye molecules were excited to their excited states. The emissions decayed because of the existence of the intramolecular, intermolecular, and interfacial nonradiative processes. We have shown in the preceding section that the IET process occurs in ~100 fs; here, we further provide strong evidence for the IET to occur on the same time scale in the TA experiments. It is therefore reasonable to assign the TA signals observed in solid films as being due to ionic species, presumably the conduction band electrons in the TiO_2 nanoparticles[37] that were produced when electron injection occurred to form charge separation between the dye cations and the negatively charged TiO_2 nanoparticles. The slow-decay components might thus be due to charge recombination; that is, part of the electrons on TiO_2 might transfer back to the dye cations so that a slow decay was observed while the charge-separated species are still in a majority that gives the persistent TA signals observed in the long-time region. The observed τ_2 of the Ru-2/TiO_2 film is significantly smaller than that of the Ru-1/TiO_2 film (23 versus 70 ps) because the electron transfer back through bonds was also more efficient than that through space.

Conclusion

We measured time-resolved emission of two ruthenium complexes in ethanol solution and in PMMA and TiO_2 thin films. In the ethanol solution, the rate of intersystem crossing for ^{1}MLCT → ^{3}MLCT was determined to be $(\sim 140\ \text{fs})^{-1}$, and the rate of vibrational relaxation of hot ^{3}MLCT molecules was $(\sim 3.8\ \text{ps})^{-1}$. After relaxation to a cold ^{3}MLCT state, the rate of intersystem crossing from ^{3}MLCT to the ground state was $(700\ \text{ns})^{-1}$. When Ru-1 was mixed with a PMMA film, the rate of aggregation-induced self-quenching varied from $(220\ \text{ns})^{-1}$ to $(5\ \text{ns})^{-1}$. To examine the effects of interfacial electron transfer through bonds and space, we measured femtosecond emission and transient absorption spectroscopy of Ru-1 and Ru-2 on TiO_2 nanoparticles in a film; the results indicate that the rates of electron transfers through space and through bonds have similar magnitudes. Because both processes are much more rapid than charge recombination, the importance of electron transfer through space should be reconsidered in the study of dye-sensitized solar cells.

Acknowledgment. The National Science Council of Republic of China provided financial support through project contracts 95-2113-M-009-027 and 95-2120-M-009-006. The support from the MOE-ATU program is also acknowledged.

References and Notes

(1) Green, M. A.; Emery, K.; King, D. L.; Igari, S.; Warta, W. *Prog. Photovoltaics* **2004**, *12*, 365−372.

(2) (a) Hara, K.; Kurashige, M.; Dan-oh, Y.; Kasada, C.; Shinpo, A.; Suga, S.; Sayama, K.; Arakawa, H. *New J. Chem.* **2003**, *27*, 783−785. (b) Hara, K.; Sato, K.; Katoh, R.; Furube, A.; Ohga, Y.; Shinpo, A.; Suga, S.; Sayama, K.; Sugihara, H.; Arakawa, H. *Phys. Chem. B* **2003**, *107*, 597−606.

(3) Horiuchi, T.; Miura, H.; Sumioka, K.; Uchida, S. *J. Am. Chem. Soc.* **2004**, *126*, 12218−12219.

(4) Dabestani, R.; Bard, A. J.; Campion, A.; Fox, M. A.; Mallouk, T. E.; Webber, S. E.; White, J. M. *J. Phys. Chem.* **1988**, *92*, 1872−1878.

(5) (a) Luo, L.-Y.; Lo, C.-F.; Lin, C.-Y.; Chang, I.-J.; Diau, E. W.-G. *J. Phys. Chem. B* **2006**, *110*, 410−419. (b) Lo, C.-F.; Luo, L.-Y.; Diau, E. W.-G.; Chang, I.-J.; Lin, C.-Y. *Chem. Commun.* **2006**, 1430−1432.

(6) Spanggaard, H.; Krebs, F. C. *Sol. Energy Mater. Sol. Cells* **2004**, *83*, 125−146.

(7) (a) Nazeeruddin, M. K.; Kay, A.; Rodicio, R.; Humphry-Baker Miller, E.; Liska, P.; Vlachopoulos, N.; Grätzel, M. *J. Am. Chem. Soc.* **1993**, *115*, 6382−6390. (b) Grätzel, M. *Inorg. Chem.* **2005**, *44*, 6841−6851. (c) Nazeeruddin, M. K.; Angelis, F. D.; Fantacci, S.; Selloni, A.; Viscardi, G.; Liska, P.; Ito, S.; Takeru, B.; Grätzel, M. *J. Am. Chem. Soc.* **2005**, *127*, 16835−16847. (d) Wang, Q.; Ito, S.; Grätzel, M.; Fabregat-Santiago, F.; Mora-Seró, I.; Bisquert, J.; Bessho, T.; Imai, H. *J. Phys. Chem. B* **2006**, *110*, 25210−25221.

(8) Haque, S. A.; Tachibana, Y.; Klug, D. R.; Durrant, J. R. *J. Phys. Chem. B* **1998**, *102*, 1745−1749.

(9) Hirata, N.; Lagref, J.-J.; Palomares, E. J.; Durrant, J. R.; Nazeeruddin, M. K.; Grätzel, M.; Censo, D. D. *Chem.—Eur. J.* **2004**, *10*, 595−602.

(10) Ellingson, R. J.; Asbury, J. B.; Ferrere, S.; Ghosh, H. N.; Sprague, J. R.; Lian, T.; Nozik, A. J. *J. Phys. Chem. B* **1998**, *102*, 6455−6458.

(11) (a) Tachibana, Y.; Moser, J. E.; Grätzel, M.; Klug, D. R.; Durrant, J. R. *J. Phys. Chem.* **1996**, *100*, 20056−20062. (b) Tachibana, Y.; Haque, S. A.; Mercer, I. P.; Durrant, J. R.; Klug, D. R. *J Phys. Chem. B* **2000**, *104*, 1198−1205.

(12) (a) Kallioinen, J.; Benkö, G.; Sundström, V.; Korppi-Tommola, J. E. I.; Yartsev, A. P. *J. Phys. Chem. B* **2002**, *106*, 4396−4404. (b) Benkö, G.; Kallioinen, J.; Myllypenkiö, P.; Trif, F.; Korppi-Tommola, J. E. I.; Yartsev, P., A.; Sundström, V. *J. Phys. Chem. B* **2004**, *108*, 2862−2867.

(13) Wenger, B.; Grätzel, M.; Moser, J.-E. *J. Am. Chem. Soc.* **2005**, *127*, 12150−12151.

(14) Damrauer, N. H.; Cerullo, G.; Yeh, A.; Boussie, T. R.; Shank, C. V.; McCusker, J. K. *Science* **1997**, *275*, 54−57.

(15) Bhasikuttan, A. C.; Suzuki, M.; Nakashima, S.; Okada, T. *J. Am. Chem. Soc.* **2002**, *124*, 8398−8405.

(16) Kallioinen, J.; Benkö, G.; Myllyperkiö, P.; Khriachtchev, L.; Skårman, B.; Wallenberg, R.; Tuomikoski, M.; Korppi-Tommola, J.; Sundström, V.; Yartsev, A. P. *J. Phys. Chem. B.* **2004**, *108*, 6365−6373.

(17) Hara, K.; Houriuchi, H.; Katoh, R.; Singh, L. P.; Sugihara, H.; Sayama, K.; Murata, S.; Tachiya, M.; Arakawa, H. *J. Phys. Chem. B* **2002**, *106*, 374−379.

(18) Kilså, K.; Mayo, E. I.; Brunschwig, B. S.; Gray, H. B.; Lewis, N. S.; Winkler, J. R. *J. Phys. Chem. B* **2004**, *108*, 15640−15651.

(19) Sprintschnik., G.; Sprintschnik, H. W.; Kirsch, P. P.; Whitten, D. G. **1977**, *99*, 4947−4953.

(20) Barbé, C. J.; Arendse, F.; Comte, P.; Jirousek, M.; Lenzmann, F.; Shklover, V.; Grätzel, M. *J. Am. Ceram. Soc.* **1997**, *80*, 3157−3171.

(21) (a) Bhongale, C. J.; Chang, C.-W.; Lee, C.-S.; Diau, E. W.-G.; Hsu, C.-S. *J. Phys. Chem. B* **2005**, *109*, 13472−13482. (b) Bhongale, C. J.; Chang, C.-W.; Diau, E. W.-G.; Hsu, C.-S.; Dong, Y.; Tang, B.-Z. *Chem. Phys. Lett.* **2006**, *419*, 444−449. (c) Lin, J.-S.; Chen, Y.-C.; Chen, C.-C.; Luo, L.-Y.; Diau, E. W.-G.; Liu, T.-F. *J. Chin. Chem. Soc.* **2006**, *53*, 1405−1412.

(22) (a) Lu, Y.-C.; Chang, C.-W.; Diau, E. W.-G. *J. Chin. Chem. Soc.* **2002**, *49*, 693−701. (b) Lu, Y.-C.; Diau, E. W.-G.; Rau, H. *J. Phys. Chem. A* **2005**, *109*, 2090. (c) Chang, C.-W.; Lu, Y.-C.; Wang, T.-T.; Diau, E. W.-G. *J. Am. Chem. Soc.* **2004**, *126*, 10109−10118.

(23) Wallin, S.; Davidsson, J.; Modin, J.; Hammarström, L. *J. Phys. Chem. A* **2005**, *109*, 4697−4704.

(24) Barigelletti, F.; Juris, A.; Balzani, V.; Belser, P.; Zelewsky, A. V. *Inorg. Chem.* **1983**, *22*, 3335−3339.

(25) Auweter, H.; Haberkorn, H.; Heckmann, W.; Horn, D.; Lüddecke, E.; Rieger, J.; Weiss, H. *Angew. Chem., Int. Ed.* **1999**, *38*, 2188−2191.

(26) Houten, J. V.; Watts, R. J. *J. Am. Chem. Soc.* **1976**, *98*, 4853−4858.

(27) Fan, J.; Tysoe, S.; Strekas, T. C.; Gafney, H. D.; Serpone, N.; Lawless, D. *J. Am. Chem. Soc.* **1994**, *116*, 5343−5351.

(28) Chang, C.-W.; Kao, Y.-T.; Diau., E. W.-G. *Chem. Phys. Lett.* **2003**, *374*, 110−118.

(29) Glasbeek, M.; Zhang, H. *Chem. Rev.* **2004**, *104*, 1929−1954.

(30) Wang, T.-T.; Chung, S.-M.; Wu, F.-I.; Shu, C.-F.; Diau, E. W.-G. *J Phys. Chem. B* **2005**, *109*, 23827−23835.

(31) Ogawa, M.; Nakamura, T.; Mori, J.-I.; Kuroda, K. *J. Phys. Chem. B* **2000**, *104*, 8554−8556.

(32) Hashimoto, K.; Hashimoto, M.; Lever, A. B. P.; Sakata, T. *J. Phys. Chem.* **1988**, *92*, 1016−1018.

(33) Clark, W. D. K.; Sutin, N. *J. Am. Chem. Soc.* **1977**, *99*, 4676−4682.

(34) Luo, L.; Chang, C.-W.; Lin, C.-Y.; Diau, E. W.-G. *Chem. Phys. Lett.* **2006**, *432*, 452−456.

(35) Wasielewski., M. R. *Chem. Rev.* **1992**, *92*, 435−461.

(36) Turro, N. J. *Modern Molecular Photochemistry*; University Science Books: Sausalito, CA, 1978.

(37) Ramakrishna, G.; Jose, D. A.; Kumar, D. K.; Das, A.; Palit, D. K.; Ghosh, H. N. *J. Phys. Chem. B* **2005**, *109*, 15445−15453.